The Astrophysical Journal, 780:27 (15pp), 2014 January 1 doi:10.1088/0004-637X/780/1/27

THE RANGE OF VARIATION OF THE MASS OF THE MOST MASSIVE STAR IN STELLAR CLUSTERS DERIVED FROM 35 MILLION MONTE CARLO SIMULATIONS

Bogdan Popescu and M. M. Hanson
Department of Physics, University of Cincinnati, P.O. Box 210011, Cincinnati, OH 45221-0011, USA;
bogdan.popescu@uc.edu, margaret.hanson@uc.edu
Received 2013 July 2; accepted 2013 October 28; published 2013 December 10

ABSTRACT

A growing fraction of simple stellar population models, in an aim to create more realistic simulations capable of including stochastic variation in their outputs, begin their simulations with a distribution of discrete stars following a power-law function of masses. Careful attention is needed to create a correctly sampled initial mass function (IMF), and here we provide a solid mathematical method, called MASSCLEAN IMF Sampling, for doing so. We use our method to perform *10 million* MASSCLEAN Monte Carlo stellar cluster simulations to determine the most massive star in a mass distribution as a function of the total mass of the cluster. We find that a maximum mass range is predicted, not a single maximum mass. This range is (1) dependent on the total mass of the cluster and (2) independent of an upper stellar mass limit, M_{limit}, for *unsaturated* clusters and emerges naturally from our IMF sampling method. We then turn our analysis around, starting with our new database of *25 million* simulated clusters, to constrain the highest mass star from the observed integrated colors of a sample of 40 low-mass Large Magellanic Cloud stellar clusters of known age and mass. Finally, we present an analytical description of the maximum mass range of the most massive star as a function of the cluster's total mass and present a new M_{max}–$M_{cluster}$ relation.

Key words: open clusters and associations: general – galaxies: clusters: general – methods: analytical

Online-only material: color figures

1. INTRODUCTION

It is indeed fortunate that one of the most fundamental of astrophysical distribution functions, the initial mass function (IMF), is described by such a simple equation as a power law. Yet this power law, describing the number of stars formed as a function of mass, or the stellar mass spectrum, is central to a broad set of fields in astrophysics. It is applicable to studies of our solar neighborhood and estimating the number of habitable planets as well as to estimating the mass of the most distant galaxies. This is possible not just because it is so easily expressed mathematically, but because its functional form is virtually universal and, thus, applicable for studies near and far, past and present. Currently, Salpeter's (1955) original paper first reporting the relationship garners over 300 citations per year, making it among the most cited historical publications in all of astronomy. Kroupa (2001), which provides the most accurate present-day values for the exponents used in that power law as a function of mass range, yields another 200 references per year. The IMF touches, and is deeply fundamental to, virtually all fields of astrophysics. If our use or the analysis of the IMF were in some way wrong or biased, it would have a profound impact on our science.

The apparent simplicity of a power-law equation can be deceiving. For instance, when attempting to derive the IMF for a population of stars, biases can be introduced in the calculation of the IMF slope for a population of stars because of the use of constant bin sizes. In such an analysis, the bins for high-mass stars may have very few stars, while bins counting lower mass stars may have tens, hundreds, or even thousands of stars. The bias occurs as a result of inappropriate weighting of the bins when χ^2 minimization is used to fit the slope. This has has been pointed out by many, starting over a decade ago (Kroupa 2001; Elmegreen 2004; Maíz Apellániz & Úbeda 2005).

What has only more recently been fully recognized is the bias introduced when the IMF is used to derive a distribution of stars, such as when creating simulations of a stellar cluster or a galaxy. In some of the earliest models, broadly referred to as simple stellar population (SSP) models (e.g., Bruzual & Charlot 2003), bin size was not a problem because all bins were deemed equal. These models assumed an *infinite* mass was available for their stellar distribution. In this kind of analysis, the bins represented the fractional, probabilistic portion compared with the entire stellar distribution. The amount of light or total mass coming from those bins was simply proportional based on this fractional distribution as dictated by stellar evolutionary isochrones. A bias due to variable weighting was not an issue, because discrete stars were not being created. However, such an analysis cannot be extended to model the observed properties of low-mass or even mid-mass clusters. Such models will predict nonphysical values for cluster magnitudes and colors with age, for example, calling for a fractional O star.

If one wishes to simulate a more realistic stellar cluster, down to the tracking of individual stars, and if that cluster is of moderate to low mass (less than $10^4\ M_\odot$), then assigning stars statistically from a power-law distribution will require real, *whole* stars. This also means that bin size must be considered, and possible forms of bias need to be identified and addressed.

In this contribution, we explore the challenges faced with ensuring that we create stellar cluster simulations that produce discrete samples of whole stars that fully obey a power-law IMF, but that also assign masses in such a way that the binning does not lead to any biases in IMF slope or stellar mass range. This latter quality will be critical for investigating whether observed clusters in the Large Magellanic Cloud (LMC) show evidence for a upper mass stellar limit M_{limit}, or if stellar cluster mass imposes a genuine and biased limit on the most massive star, M_{max}, it can form.

We begin by describing our method to fill the IMF, called MASSCLEAN IMF Sampling. In Section 2, we describe the differences between our method and two others: random sampling and optimal sampling (Kroupa et al. 2011). In Section 3, we describe how MASSCLEAN generates the most massive star in the mass distribution of stellar clusters and compare it with previous work in the field. In Section 4, we present the range of variation of the mass of the most massive star as a function of cluster's mass determined from *10 million* Monte Carlo simulations. We present our new method of deriving the mass of the most massive star using the integrated colors and magnitudes and *25 million* Monte Carlo simulations in Section 5. This method is used to estimate the mass of the most massive star for 40 LMC clusters. In Section 6, we present an analytical description of the mass range for the most massive star, as well as for the M_{max}–$M_{cluster}$ relation. Concluding remarks are given in Section 7.

2. MASSCLEAN IMF SAMPLING

The original theory for the IMF was created, developed, and tested using observational data. When they were available, the masses of the stars, which form a *discrete* distribution, were used to fit a *continuous* power law (or multi–power law). The most convenient way for this to be achieved was to use constant-mass bins. Another method for measuring the IMF is based on obtaining the *K*-band luminosity function. Here, the convenient way of calculating such a function requires setting up constant-magnitude bins, which then translate into variable-mass bins. So, from the observational point of view, fitting a *discrete* distribution to a continuous power law can be independent of the choice of bins.

However, doing the opposite, filling the *continuous* IMF function to obtain a *discrete* distribution of stars, comes with a whole new set of challenges. Traditional population synthesis models (e.g., Bruzual & Charlot 2003; Marigo et al. 2008) were computed in the *infinite mass limit*, by assigning a different probability to the stars filling the isochrone. While this works for very massive stellar clusters, for clusters of more typical mass this corresponds to unphysical, fractional stars, mostly at the upper end of the IMF (e.g., Popescu & Hanson 2010b; Popescu et al. 2012). An alternative method is to randomly populate the IMF. This method will clearly produce a *discrete* distribution. However, as with the binning problem identified in measuring the IMF in clusters, this method will lead to incorrectly populating the cluster, as was shown by Kroupa et al. (2011) and we demonstrate here.

For our IMF sampling, we will use our analysis package, MASSCLEAN[1] (Popescu & Hanson 2009). A thorough description of the code is available from our earlier papers (Popescu & Hanson 2009, 2010a, 2010b; Popescu et al. 2012), but perhaps most unique is that it allows for a realistic representation of the stochastic fluctuations that occur in real clusters, which is increasingly important as the mass of the cluster decreases. We provide an outline of the critical aspects of the simulation that apply to this investigation below.

The mass distribution of stars in stellar clusters is described by the IMF, so the number of stars formed in the $M \pm dM$ range is

$$dN = \xi(M) dM\,, \tag{1}$$

where $\xi(M)$ is the Kroupa–Salpeter IMF (Kroupa 2001, 2002; Kroupa et al. 2011; Salpeter 1955):

$$\xi(M) = k \begin{cases} \left(\frac{M}{m_1}\right)^{-\alpha_1}, & m_0 < M \leqslant m_1\,, \\ \left(\frac{M}{m_1}\right)^{-\alpha_2}, & m_1 < M \leqslant m_2\,, \\ \left(\frac{m_2}{m_1}\right)^{-\alpha_2} \left(\frac{M}{m_2}\right)^{-\alpha_3}, & m_2 < M \leqslant m_3\,, \end{cases} \tag{2}$$

with mass expressed in units of $M_\odot$. For this work, we used

$$\begin{aligned} \alpha_1 &= +0.30, \quad 0.01 \leqslant M/M_\odot < 0.08\,, \\ \alpha_2 &= +1.30, \quad 0.08 \leqslant M/M_\odot < 0.50\,, \\ \alpha_3 &= +2.35, \quad 0.50 \leqslant M/M_\odot < m_3\,, \end{aligned} \tag{3}$$

and $m_3 = M_{cluster}$ (the total mass of the cluster) or $m_3 = M_{limit}$ (for an IMF with upper mass cutoff; e.g., Oey & Clarke 2005; Kroupa et al. 2011). Note that for $\alpha_1 = \alpha_2 = \alpha_3 = 2.35$, $\xi(M)$ becomes the Salpeter (1955) IMF.

Using $\xi(M)/k = \xi_i(M)$ (with $i = 1, 2, 3$), the IMF can be simplified to

$$\xi(M) = k\, \xi_i(M)\,. \tag{4}$$

Then the total mass of the cluster can be written

$$M_{cluster} = \int_0^{N_{max}} M(N) dN\,, \tag{5}$$

$$M_{cluster} = \int_{m_0}^{m_3} M \frac{dN}{dM} dM = \int_{m_0}^{m_3} \xi(M) M dM\,, \tag{6}$$

$$M_{cluster} = \sum_{i=1}^{3} \left(k \int_{m_{i-1}}^{m_i} \xi_i(M) M dM \right). \tag{7}$$

The normalization constant is

$$k = \frac{M_{cluster}}{\sum_{i=1}^{3} \left(\int_{m_{i-1}}^{m_i} \xi_i(M) M dM \right)}. \tag{8}$$

From Equations (1), (2), (4), and (8), we obtain an equation that describes each bin:

$$N_i(M, \Delta M) = \frac{M_{cluster} \int_{M-\Delta M}^{M+\Delta M} \xi_i(M) dM}{\sum_{i=1}^{3} \left(\int_{m_{i-1}}^{m_i} \xi_i(M) M dM \right)}. \tag{9}$$

Note that the sum of integrals is a constant,

$$C = \sum_{i=1}^{3} \left(\int_{m_{i-1}}^{m_i} \xi_i(M) M dM \right), \tag{10}$$

so Equation (9) can be written

$$N_i(M, \Delta M) = \frac{M_{cluster}}{C} \int_{M-\Delta M}^{M+\Delta M} \xi_i(M) dM. \tag{11}$$

Equation (11) could be used to compute the number of stars in any mass interval, as described in Popescu & Hanson (2009). It could also be used to compute the probabilities or the multiplicative factors corresponding to isochrone stars used in traditional SSP models computed in the *infinite mass limit* (e.g., Marigo et al. 2008; Girardi et al. 2010).

[1] See http://www.physics.uc.edu/~popescu/massclean/. The **MASS**ive **Cl**uster **E**volution and **AN**alysis package is publicly available under GNU General Public License (© 2007–2013 by Bogdan Popescu and Margaret Hanson).

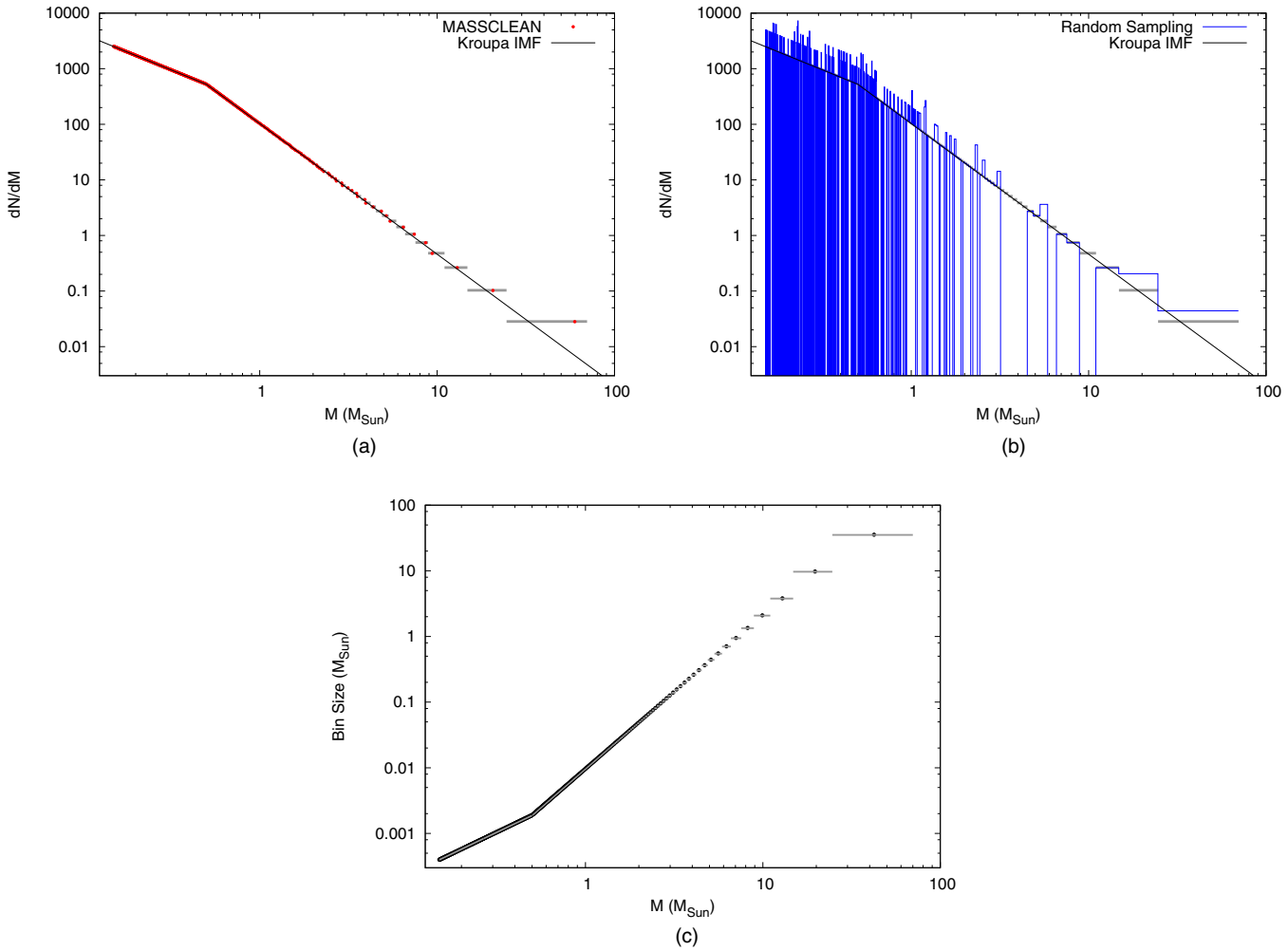

Figure 1. Stellar IMF. (a) The diagonal line represents the Kroupa–Salpeter IMF as given in Equation (2). The segmented horizontal lines represent the variable-mass bins created using our MASSCLEAN IMF Sampling (MIMFS) method, assuming a total cluster mass of 500 $M_{\odot}$. Discrete stars are shown by red dots, with one per MIMFS mass bin. (b) Same as (a), but overlaid in blue is the result of a stellar distribution created using a randomly populated IMF, leaving numerous gaps. (c) The mass-dependent bins of the MIMFS method.

(A color version of this figure is available in the online journal.)

However, if we wish to create a *discrete* distribution of stars in a cluster, it cannot include a *fractional* number of stars. Thus, the challenge is to compute the M_{j-1} and M_j mass limits such that $N_i(M_{j-1}, M_j)$ will always give an integer value. Kroupa et al. (2011) describe a similarly derived set of equations and force each bin to contain precisely 10 stars. They call this OPTIMAL SAMPLING, where the IMF is perfectly sampled without any gaps in the distribution and the stellar masses are ideally spaced. They suggest that this is a more realistic approach to populating the IMF as compared with the more traditionally used random sampling of the IMF (Kroupa et al. 2011).

Using Equation (11), MASSCLEAN also computes an integer value of stars per variable-mass bin. However, for our simulations, we define each bin to include exactly one star. In other words, we set $N_i(M_{j-1}, M_j) = 1$. We call this method MASSCLEAN IMF Sampling (MIMFS). The expanded utility of this choice over the Kroupa et al. (2011) OPTIMAL SAMPLING method will become apparent soon.

Let us switch to the notation $M_j = M - \Delta M$ and $M_{j-1} = M + \Delta M$, with $j = 1$ to N_{max}. When

$$N_i(M_j, M_{j-1}) = \frac{M_{cluster}}{C} \int_{M_j}^{M_{j-1}} \xi_i(M) dM = 1\,, \qquad (12)$$

the choice of j shows that bin (M_j, M_{j-1}) contains the jth most massive star. In this notation, the most massive star in the cluster will be found in the (M_1, M_0) bin.

For another set of constants, let us use the notation $\gamma_i = \xi_i(M)/M^{-\alpha_i}$ (with $i = 1, 2, 3$). From Equation (12), we can compute M_j:

$$M_j = \left(M_{j-1} - \frac{C}{M_{cluster}} \frac{1-\alpha_i}{\gamma_i} \right)^{\frac{1}{1-\alpha_i}}. \qquad (13)$$

Consequently, the interval (M_{j-1+N}, M_{j-1}) will contain N stars, with

$$M_{j-1+N} = \left(M_{j-1} - \frac{CN}{M_{cluster}} \frac{1-\alpha_i}{\gamma_i} \right)^{\frac{1}{1-\alpha_i}}. \qquad (14)$$

In Figure 1(a), we show an example demonstrating the MIMFS method for distributing stars, for a stellar cluster with $M_{cluster} = 500\,M_{\odot}$. The Kroupa (2001) IMF is presented as the diagonal black line, and the (M_j, M_{j-1}) MASSCLEAN variable-mass bins are displayed as horizontal gray lines. The mass values for all of the stars created as part of this cluster from a sample MASSCLEAN run are shown as red dots. This

sample mass distribution is consistent with the continuous IMF power law. However, it also includes very real fluctuations, as the stellar mass M is allowed to fall anywhere in the (M_j, M_{j-1}) bin. Although the fluctuations of the red dots from the line representing the Kroupa (2001) IMF value may appear small, they can generate a large dispersion in the integrated magnitudes and colors of simulated clusters and are consistent with available observational data (Popescu & Hanson 2010a, 2010b; Popescu et al. 2012). This is because the fluctuations (allowed mass range) within each bin is proportional to the bin mass, with the highest mass fluctuations occurring among the most massive stars in the cluster. The MIMFS method correctly simulates the largest variation in integrated magnitude and color as being seen among the low-mass clusters, as they have relatively few, very large bins at the high-mass end.

In Figure 1(b), we present an example mass distribution generated using the traditional random sampling of the IMF with the same 500 $M_\odot$ stellar cluster. To compare with the MIMFS method, we also plot the same grayscale lines representing MASSCLEAN bins as presented in Figure 1(a). As already pointed out by Kroupa et al. (2011), the traditional method of random sampling shows large variations from the IMF, with many large gaps. As discussed above, these unnatural variations will not disappear simply by virtue of using a different choice of bin size. While random sampling will work in the realm of deriving *relative* fractional stars in the limit of an *infinite mass* distribution, it cannot be used to populate an IMF properly when a discrete stellar distribution is needed, such as when simulating low-mass clusters (Maíz Apellániz 2009).

Note that in both Kroupa et al.'s (2011) OPTIMAL SAMPLING and our own MIMFS method, the bin size will be mass dependent. The size of the bins as a function of mass is presented in Figure 1(c). The bin size $\Delta M_{\rm bin} = M_{j-1} - M_j$ is expressed on the vertical axes as black dots. The limits of the bins are represented along the horizontal axis by the gray lines. The plot shows that $log(\Delta M_{bin}) \propto log(M)$. Moreover, as described by Equation (13), the bin size also depends on the mass of the cluster, $M_{cluster}$. This is an obvious result if one recalls that we are forcing each bin to hold just one star. More massive clusters will have proportionally more bins over the same stellar mass range.

Figure 2 is an example of a K-band luminosity function derived using our MIMFS method. The sample cluster presented in Figure 2 was simulated with MASSCLEAN and is 1 million years old, with $M = 500\,M_\odot$. The slope in the histogram depends on the mass-to-light ratio and on the α_3 value. It can also be used to constrain the stellar IMF. The constant-magnitude bins in the histogram (labeled on the bottom axis) correspond to logarithmic, age-dependent bins in mass (labeled on the top axis).

3. THE MOST MASSIVE STAR IN A STELLAR CLUSTER

There are strong similarities between Kroupa et al.'s (2011) OPTIMAL SAMPLING and our MIMFS method for discretely populating stellar clusters: the bins are mass dependent, and the number and bin sizes are dependent on the cluster mass. This leads to a stellar mass distribution that truly obeys the IMF. But there is one significant difference in the two methods. By forcing our bins in the MIMFS method to contain no more than one star, we are able to go one step further and make analytical predictions for the mass of the most massive star in a cluster.

Following the formalism and notation presented in Section 2, the most massive star in the mass distribution can be described

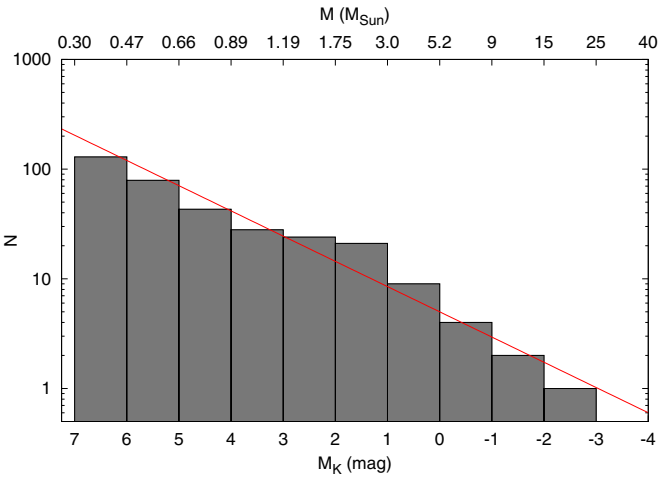

Figure 2. K-band luminosity function derived using MIMFS for a $M = 500\,M_\odot$ cluster, 10^6 yr old.

(A color version of this figure is available in the online journal.)

using Equation (12):

$$\frac{M_{cluster}}{C}\int_{M_1}^{M_0}\xi_3(M)dM = N_3(M_1, M_0) = 1, \quad (15)$$

$$M_{cluster}\frac{\gamma_3}{C}\int_{M_1}^{M_0}M^{-\alpha_3}dM = N_3(M_1, M_0) = 1. \quad (16)$$

For the upper limit, we will start with three choices: $M_0 = \infty$ (e.g., Elmegreen 2000; for the convenience of the computation and description); $M_0 = M_{cluster}$ (since the most massive star obviously cannot have a mass larger than the entire cluster mass); and $M_0 = M_{limit}$ (the maximum stellar mass; e.g., Oey & Clarke 2005).

When $M_0 = \infty$, M_1 can be determined from Equation (16):

$$M_1 = \left(\frac{\gamma_3}{C}\frac{1}{\alpha_3 - 1}\right)^{\frac{1}{\alpha_3-1}} M_{cluster}^{\frac{1}{\alpha_3-1}}. \quad (17)$$

Adding numbers, this simplifies to

$$M_1 = 0.2375\ M_{cluster}^{\frac{1}{1.35}}. \quad (18)$$

This is virtually identical to the relation found by Elmegreen (2000), who used a similar formalism but a different IMF:

$$M_{max} = 100\left(\frac{M_{cluster}}{3\times 10^3}\right)^{\frac{1}{1.35}}. \quad (19)$$

Both M_1 and M_{max} given by Equations (18) and (19), respectively, are proportional to $M_{cluster}^{\frac{1}{1.35}}$.

When the upper mass limit is changed to $M_0 = M_{cluster}$, from Equation (16) we instead have

$$M_1 = \left(M_{cluster}^{1-\alpha_3} - \frac{C}{M_{cluster}}\frac{1-\alpha_3}{\gamma_3}\right)^{\frac{1}{1-\alpha_3}}. \quad (20)$$

Again, adding numbers this simplifies to

$$M_1 = \left(M_{cluster}^{-1.35} - \frac{6.9653}{M_{cluster}}\right)^{-\frac{1}{1.35}}. \quad (21)$$

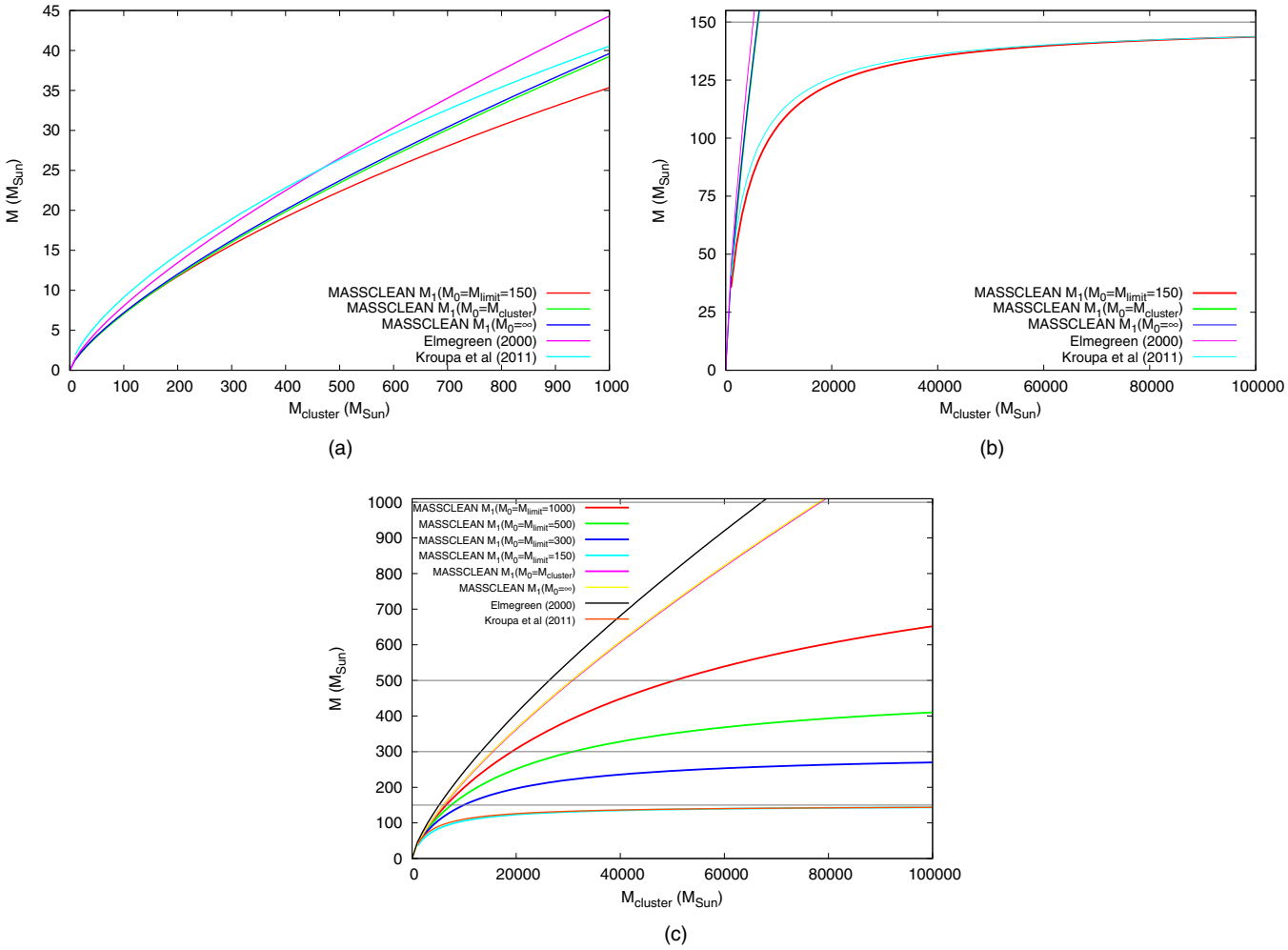

Figure 3. Graphical representations of the most massive star possible in a cluster versus the cluster total mass, using the different expressions discussed in Section 3. (a) For modest cluster masses, $M_{cluster} < 1000\,M_{\odot}$, the limit chosen for the most massive star has a somewhat minor effect on the predicted most massive star observed in the host cluster. (b) Once the cluster mass becomes fairly large, and beyond 10,000 $M_{\odot}$, an increasingly large divergence is seen in the predicted maximum mass and between expressions that allow an infinite stellar mass and those limiting the stellar mass. (c) A closer look at the predicted maximum stellar mass, based on differing upper mass limits, from $M_{max} = 150\,M_{\odot}$ through 1000 $M_{\odot}$.

(A color version of this figure is available in the online journal.)

Although it seems reasonable to use $M_{cluster}$ as an upper mass limit instead of ∞, the difference between Equations (18) and (21) is indeed very small. Figure 3(a) shows the shapes of these two functions. They are virtually identical, with $M_0 = \infty$ predicting only a slightly more massive star formed in the corresponding cluster.

Changing the upper mass limit to a specific upper mass maximum value M_{limit} in Equation (16) gives

$$M_1 = \left(M_{limit}^{1-\alpha_3} - \frac{C}{M_{cluster}} \frac{1-\alpha_3}{\gamma_3} \right)^{\frac{1}{1-\alpha_3}}. \quad (22)$$

After simplifying the numbers, this leads to

$$M_1 = \left(M_{limit}^{-1.35} - \frac{6.9653}{M_{cluster}} \right)^{-\frac{1}{1.35}}. \quad (23)$$

This expression is close to Kroupa et al. (2011), who found

$$\log(M_{max}) = 2.56 \log(M_{cluster}) \times [3.82^{9.17} + \log(M_{cluster})^{9.17}]^{-\frac{1}{9.17}} - 0.38 \quad (24)$$

and applied a canonical upper mass limit of $M_{limit} = 150\,M_{\odot}$.

The M_1 variation described by Equations (18), (20), and (21), along with the M_{max} variation from Elmegreen (2000) and Kroupa et al. (2011), given by Equations (19) and (24), respectively, are presented in Figure 3. In Figure 3(a), the maximum mass of the cluster is 1000 $M_{\odot}$. In this mass range, there is a fairly small difference between all of the mentioned variations for setting the upper mass limit. In the case of M_1, as noted above, there is a negligible difference when switching from $M_0 = \infty$ to $M_0 = M_{cluster}$.

In Figure 3(b), the mass range is now expanded to 100,000 $M_{\odot}$. It is now easy to see that M_{max} from Elmegreen (2000) and M_1 as given by our Equations (18) and (20) continue to agree yet quickly diverge from the other functions. As expected, Kroupa et al. (2011) and Equation (23), with $M_{limit} = 150\,M_{\odot}$, remain in good agreement over this entire range.

In Figure 3(c), the y-axis range is expanded to show the variation found in deriving M_1, given by Equation (23), for differing values for the upper mass maximum value, using limiting values of $M_{lim} = 150$, 300, 500, and 1000 $M_{\odot}$.

Both Elmegreen (2000) and Kroupa et al. (2011) use the notation M_{max} in Equations (19) and (24), respectively. Using a similar formalism, we introduced M_1 in Equations (18), (21), and (23). Obviously, the most massive star, with mass M_{max}, is most likely to be in the interval (M_1, M_0). M_1 is only a measure of the *lower mass limit* of the most massive star. M_{max}, the most massive star, could have a mass as high as M_0. When the mass of the cluster is high enough, M_0, the highest mass possible for the star, will hit the limit of the upper mass maximum value, M_{limit}. These clusters are referred to as *saturated* (Kroupa et al. 2011). For lower mass clusters, when M_{limit} is not reached, M_0 will have a range of variation depending on the total mass of the cluster, $M_{cluster}$, as discussed in the following sections.

How does the MIMFS method differ from the OPTIMAL SAMPLING of Kroupa et al. (2011)? In both cases, the IMF is filled properly (Figure 1(a)), and the bins, for *one star* (MIMFS) or *some constant integer number of stars* (OPTIMAL SAMPLING), are both mass dependent and cluster mass dependent (Figures 1(a) and (c)). However, the treatment of the most massive star is different. With OPTIMAL SAMPLING, a limit on the mass of the most massive star is used, a single-valued M_{max}–$M_{cluster}$ relation, computed for $M_{limit} = 150\,M_\odot$ (the *canonical limit*, Equation (24)).

The MIMFS method does not use a predefined, canonical, maximum mass limit for the most massive star, even for those clusters with too low a mass to expect a star to be found above the physical limit (*unsaturated clusters*). Instead, each star's mass M_k is simply assigned randomly in the interval (M_j, M_{j-1}) (Equations (12) and (13)). The upper limit of the mass of the most massive star in the cluster will be given by

$$M_0 = M_{cluster} - \sum_{k=1}^{N_{max}-1} M_k\,. \tag{25}$$

M_0 is the maximum available mass for the most massive star and depends on the entire distribution of stars. Our *10 million* Monte Carlo simulations show that M_{max} could be significantly *higher* than the *canonical limit* used by Kroupa et al. (2011), which is well approximated by M_1 (Equation (23)).

However, as a consequence of the stochastic fluctuations in each mass bin, M_{max} could also be *lower* than M_1. This is because the remaining mass for the most massive star (Equation (25)) could be lower than M_1 for *unsaturated* clusters. This is related to the way the bins are filled with the MIMFS method. Nearly all of the bins, particularly for a small cluster, will populate the distribution with very low mass stars. That any bin would be assigned a star is equally likely (the size of the bin has been specifically created to match the form of the IMF). In *unsaturated* clusters, if the highest mass bin is not filled until after most of the low-mass bins have been populated, it may not be possible to fill that bin, because the mass left for stars is less than M_1. In this situation, Equation (14) shows that the interval $(M_2, M_0 = M_{limit})$ contains $N = 2$ most massive stars:

$$M_2 = \left(M_{limit} - \frac{2C}{M_{cluster}}\frac{1-\alpha_3}{\gamma_3}\right)^{\frac{1}{1-\alpha_3}}. \tag{26}$$

Although this is a rare event, the two most massive stars could instead be located in the combined (M_2, M_{limit}) bin. So, M_2 could also be used as a measure of the lower limit of M_{max} for low-mass, *unsaturated* clusters.

4. MASS RANGE OF THE MOST MASSIVE STAR AS A FUNCTION OF CLUSTER MASS

It is reasonable to assume there is a genuine, maximum mass of a star, M_{limit}, based on the physical processes that allow for a structurally stable star (Stothers 1992; Baraffe et al. 2001; Massey 2011). At present, models of stellar structure are not able to provide a strong constraint on this limit. However, using star counts and statistical arguments, a canonical value of $M_{limit} \sim 150\,M_\odot$ has been claimed (e.g., Weidner & Kroupa 2004; Oey & Clarke 2005). This limit has also been argued based on observations made of the most massive stars in the very young, high-mass clusters *R136* in the LMC (Selman et al. 1999) and the *Arches* cluster near the center of the Milky Way (Figer 2005).

However, there have recently emerged some refinements concerning the accepted masses of the most massive stars in these clusters. Crowther et al. (2010) applied a modified spectral analysis to several stars in *NGC 3603*, the *Arches*, and *R136* and conclude that the stellar mass for some of these stars exceeds the *canonical* limit of $150\,M_\odot$. Obtaining masses of high-mass stars from atmospheric analysis is a tricky business, particularly at extremely high mass. Moreover, there is considerable evidence to suggest that stellar masses derived using spectroscopic analysis may underestimate the mass of high-mass stars, the so-called mass discrepancy problem first pointed out by Herrero et al. (1992). Regrettably, there are few high-mass binaries with extreme masses of 120 or even $150\,M_\odot$ to help calibrate these analyses (but note the recent identification that *R144* in *30 Doradus* is a binary of combined mass nearing $400\,M_\odot$; e.g., Sana et al. 2013).

We have used MASSCLEAN to perform *10 million* Monte Carlo simulations in order to determine M_{max} as a function of $M_{cluster}$. We investigate the properties of stellar clusters with the stellar mass limit M_{limit} set to 150, 300, 500, and $1000\,M_\odot$, and as part of a cluster of mass between 10 and $100{,}000\,M_\odot$. The mass distribution was computed using the MIMFS algorithm, described in Sections 2 and 3, and thus the IMF is always filled properly without any gaps. However, because of natural, stochastic fluctuations in the IMF, the mass of the most massive star, M_{max}, is not single valued. Instead, because of the use of the MIMFS method, we derive the expected *mass range* for the most massive star in a cluster.

Our results from the *10 million* Monte Carlo simulations are presented in Figures 4–6. The mass range of the most massive star, M_{max}, as a function of the cluster mass, $M_{cluster}$, is presented in Figure 4(a) as the gray-shaded area. This figure shows the stellar mass range when adhering to the canonical upper mass limit of $M_{limit} = 150\,M_\odot$. As described above, the Elmegreen (2000) maximum mass (green line; Equation (18)) and our Equation (21) (black line) will diverge at large enough cluster mass. In blue we plot Equation (23), with $M_1(M_{limit} = 150\,M_\odot)$. This resembles very well the canonical form of Kroupa et al. (2011), displayed as the cyan line. Note the blue line is not aligned with the bottom of the gray-shaded M_{max} region. This is because, as already described, sometimes the most massive star does not fall inside the massive-star bin. We show $M_2(M_{limit})$ as the red line. This represents the rare, but very real, situation in which the two most massive stars share the two top mass bins (Equation (26)). This line lies just below the lower limit of the M_{max} gray-shaded range.

In Figure 4(a), we present as the magenta line the latest fit of data from literature presented by Weidner et al. (2013)

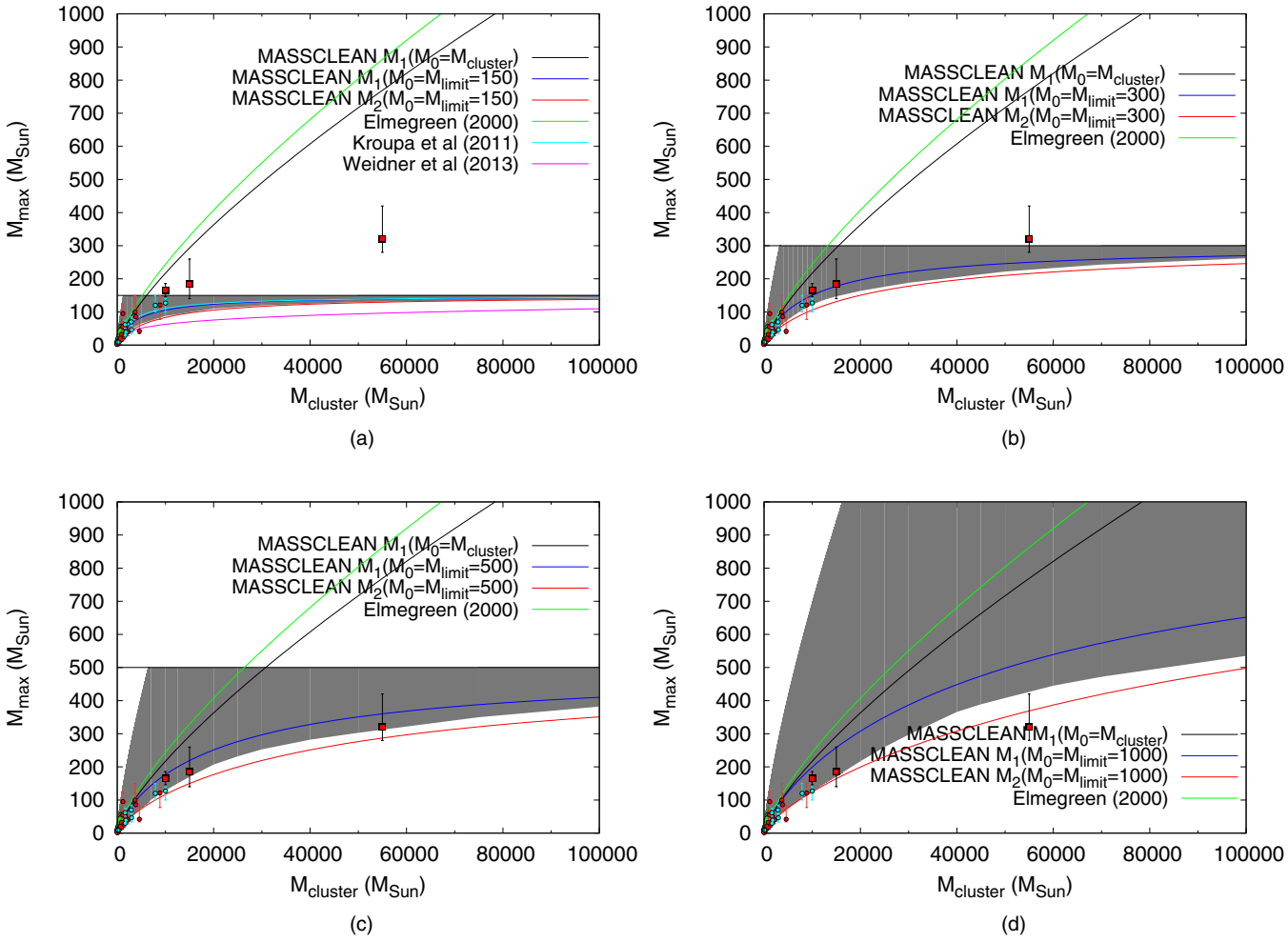

Figure 4. Mass of the most massive star, M_{max}, versus the total mass of a stellar cluster. Several analytical limits are given as solid lines. The gray-shaded regions represent MASSCLEAN simulations predicting the mass range of the most massive star expected as a function of stellar cluster mass with upper limit cutoffs of (a) 150 $M_{\odot}$, (b) 300 $M_{\odot}$, (c) 500 $M_{\odot}$, and (d) 1000 $M_{\odot}$. The observed maximum stellar mass for three clusters (in mass order: *NGC 3603*, the *Arches*, and *R136*) as derived by Crowther et al. (2010) are shown as red squares. The clusters from Weidner et al. (2010) and Weidner et al. (2013) are shown as green and red dots, respectively. Other clusters from the literature (listed in Table 1) are presented as cyan dots.

(A color version of this figure is available in the online journal.)

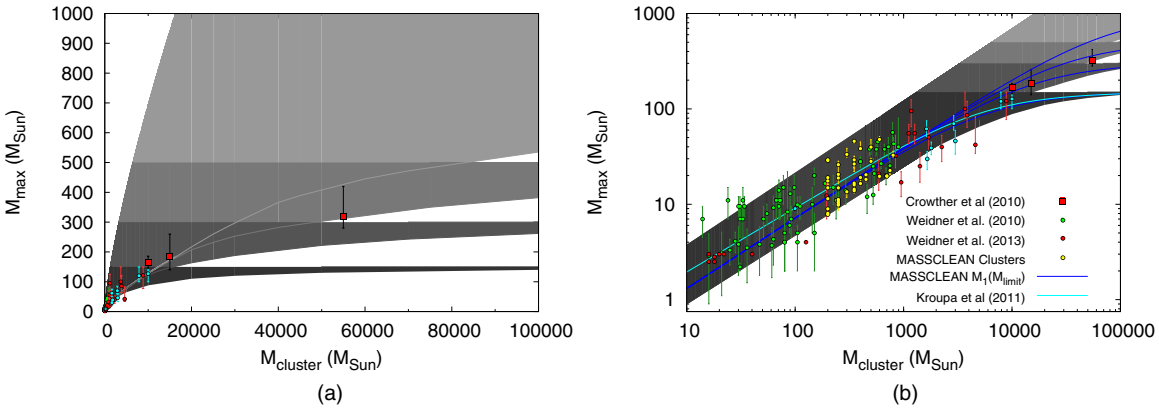

Figure 5. (a) Similar to Figure 4, but all four upper mass limits are given in a single figure with progressive gray tones. (b) Same as (a), but on a logarithmic scale. Crowther et al. (2010) clusters are shown as red squares. The clusters from Weidner et al. (2010) and Weidner et al. (2013) are shown as green and red dots, respectively. Other clusters from the literature are presented as cyan dots.

(A color version of this figure is available in the online journal.)

assuming the 150 $M_{\odot}$ *canonical limit* (their Equation (1)). This line is significantly lower than all of the other variation presented in Figure 4(a) because of the overestimation of $M_{cluster}$ at the high-mass end. For example, the *Arches* cluster is listed at over 77,000 $M_{\odot}$ in Weidner et al. (2013), while the extensive study from Clarkson et al. (2012) determined only 15,000 $M_{\odot}$. (This is also the value used in our plots; see below.) Similarly, Crowther et al. (2010) present 55,000 $M_{\odot}$ for *R136*, which is

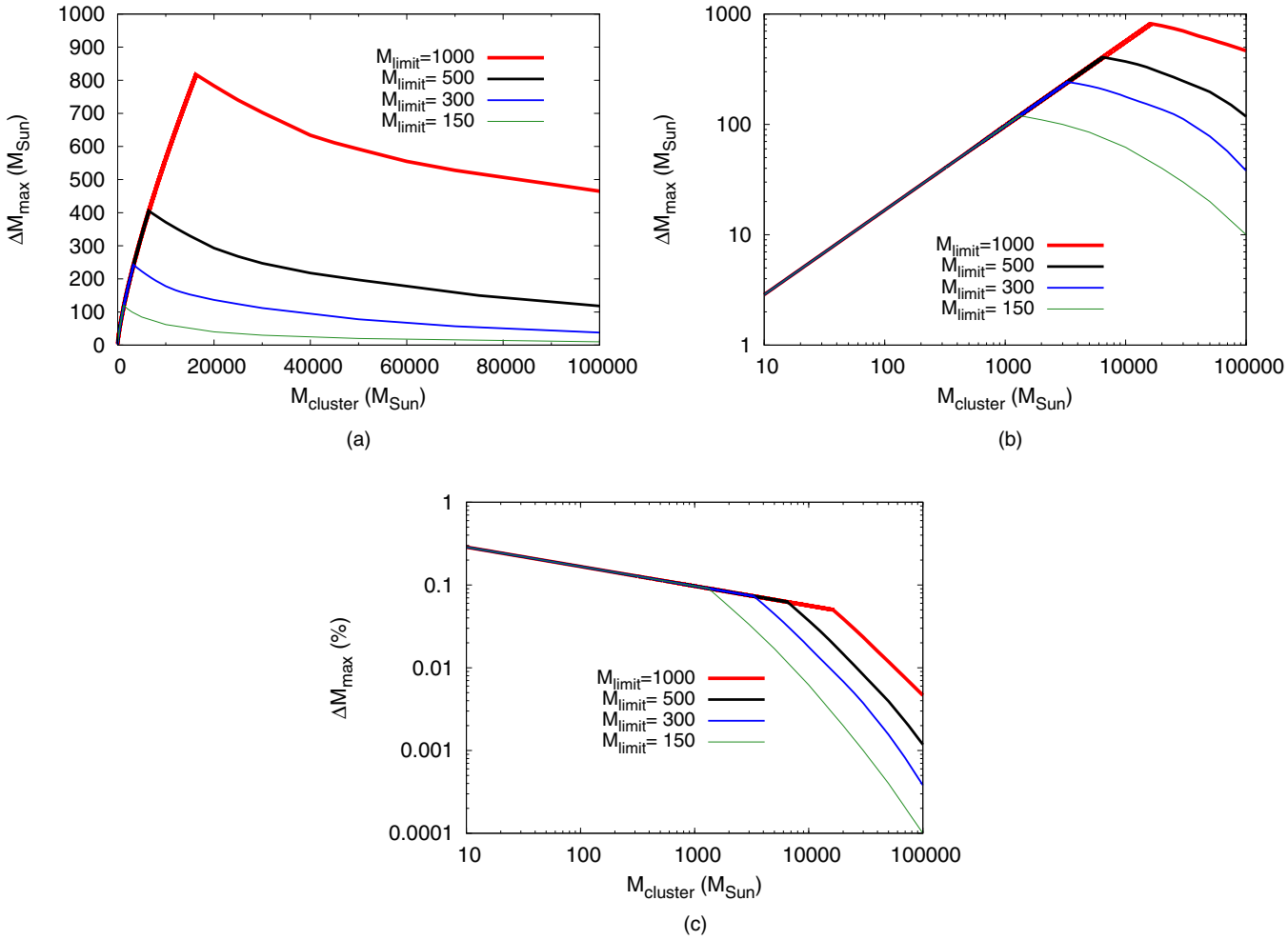

Figure 6. $\Delta M_{max} = M_{max,up} - M_{max,lo}$ versus the total mass of the cluster, $M_{cluster}$. For unsaturated clusters (up to 1000 $M_\odot$), ΔM_{max} is independent of a stellar upper mass limit. (a) Linear scale. (b) Logarithmic scale. (c) ΔM_{max} as a percentage of $M_{cluster}$.
(A color version of this figure is available in the online journal.)

significantly lower than the over 200,000 $M_\odot$ in Weidner et al. (2013).

Figures 4(b)–(d) are similar to Figure 4(a), but for $M_{limit} = 300$, 500, and 1000 $M_\odot$, respectively. The *canonical* M_{max}–$M_{cluster}$ relation of Kroupa et al. (2011) is only available for $M_{limit} = 150\,M_\odot$, but its variation is described well by the blue line (our Equation (23)) in these three figures, with the respective M_{limit}.

What should be immediately obvious from Figure 4 is that despite millions of simulations, there is a hard upper limit on the most massive star expected to be formed, and it is a function of cluster mass. Even if a million 500 $M_\odot$ clusters were sampled, our simulations indicate that a 100 $M_\odot$ star would never be formed. Yet, 100 $M_\odot$ stars are predicted to form in clusters with just 1000 $M_\odot$, although these clusters cannot form 150 $M_\odot$ stars, and so forth. What is coming out naturally from our simulations is that the lack of very high mass stars in low-mass clusters is not a sample-size effect. The upper limit on the mass of the most massive star seen being tied to the mass of the initial cluster is entirely predicted from our simulations when we properly populate the cluster's IMF.

In Figures 4(a)–(d), as a critical observational reference, we also present the locations of the most massive stars for the three massive clusters as given by Crowther et al. (2010). The three stars are shown as red squares representing $166 \pm 20\,M_\odot$ (*NGC 3603*), $185^{+75}_{-45}\,M_\odot$ (*Arches*), and $320 \pm 40\,M_\odot$ (*R136*). We also show the clusters with mass less than 1000 $M_\odot$ from Weidner et al. (2010; green dots). Additional low-mass clusters and young clusters (1 Myr) above 1000 $M_\odot$ from Weidner et al. (2013) are presented as red dots. Additional clusters from the literature (Ascenso et al. 2007; Bonatto et al. 2006; Chené et al. 2012; Crowther 2012; Davies et al. 2012; Deharveng et al. 2009; Hur et al. 2012; Martins et al. 2010) are shown as cyan dots. All of these clusters are listed in Table 1.

In Figure 5(a), we present all of the grayscale ranges from Figures 4(a)–(d) on the same plot, using four different shades of gray. Clusters from the literature are presented similarly to Figure 4. Figure 5 shows that the Crowther et al. (2010) clusters are consistent, within the error bars, with an upper stellar mass limit M_{limit} in the 300–1000 $M_\odot$ range. But Kroupa et al. (2011), citing results from Banerjee et al. (2012a, 2012b), claim these very massive stars could be so-called *supercanonical stars*, formed by the collision of massive binary stars. They use this to claim that an M_{limit} in the range of 150 $M_\odot$ cannot be excluded despite the presence of these supermassive stars. Regrettably, this is a classic circular argument. Moreover, there is no observational evidence that stars more massive than 150 $M_\odot$ must form differently, such as from mergers.

Table 1
Clusters with Values of M_{max}

Name	M ($M_\odot$)	M_{max} ($M_\odot$)	Reference[a]
1	2	3	4
NGC 3603	10000	166^{+20}_{-20}	1
Arches	15000	185^{+75}_{-45}	1, 2
R136	55000	320^{+100}_{-40}	1
IRAS 05274+3345	14^{+15}_{-7}	7.0 ± 2.5	3
Mol 139	16 ± 8	2.9 ± 2.0	3
Mol 143	21 ± 10	3.1 ± 2.0	3
IRAS 06308+0402	24^{+25}_{-13}	11.0 ± 4.0	3
VV Ser	25^{+27}_{-13}	3.3 ± 1.0	3
VY Mon	28^{+29}_{-15}	4.1 ± 1.0	3
Mol 8A	30 ± 15	3.8 ± 2.0	3
IRAS 05377+3548	30^{+32}_{-15}	9.5 ± 2.5	3
Ser SVS2	31^{+31}_{-16}	2.2 ± 0.2	3
Tau-Aur	31^{+36}_{-18}	7.0 ± 2.5	3
IRAS 05553+1631	31^{+33}_{-16}	9.5 ± 2.5	3
IRAS 05490+2658	33^{+36}_{-17}	7.0 ± 2.5	3
IRAS 03064+5638	33^{+36}_{-17}	11.0 ± 4.0	3
IRAS 06155+2319	34^{+35}_{-18}	9.5 ± 2.5	3
Mol 50	36 ± 18	3.5 ± 2.0	3
Mol 11	47 ± 20	3.8 ± 2.0	3
IRAS 06058+2138	51^{+54}_{-27}	7.0 ± 2.5	3
NGC 2023	55^{+58}_{-28}	8.0 ± 2.0	3
Mol 3	61 ± 20	3.7 ± 2.0	3
Mol 160	63 ± 20	4.3 ± 2.0	3
NGC 7129	63^{+104}_{-33}	9.2 ± 3.0	3
IRAS 06068+20303	67^{+70}_{-35}	11.0 ± 4.0	3
IRAS 00494+5617	71^{+74}_{-37}	9.5 ± 2.5	3
V921 Sco	71^{+429}_{-36}	14.0 ± 4.0	3
IRAS 05197+3355	72^{+75}_{-38}	11.0 ± 4.0	3
IRAS 05375+3540	73^{+78}_{-38}	11.0 ± 4.0	3
IRAS 02593+6016	78^{+81}_{-41}	15.0 ± 5.0	3
Cha I	80^{+91}_{-46}	5.0 ± 3.0	3
Mol 103	80 ± 20	4.0 ± 2.0	3
NGC 2071	80^{+89}_{-44}	4.0 ± 2.0	3
MWC 297	85 ± 60	$8.3^{+13.7}_{-1.3}$	3
IC 348	89^{+92}_{-46}	6.0 ± 1.0	3
BD 40° 4124	90^{+106}_{-49}	$12.9^{+2.0}_{-6.0}$	3
IRAS 06056+2131	92^{+97}_{-49}	7.0 ± 2.5	3
IRAS 05100+3723	98^{+103}_{-51}	15.0 ± 5.0	3
R CrA	105^{+114}_{-55}	4.0 ± 2.0	3
NGC 1333	105^{+111}_{-54}	5.0 ± 1.0	3
Mol 28	105 ± 20	9.9 ± 2.0	3
IRAS 02575+6017	111^{+116}_{-57}	9.5 ± 2.5	3
W40	144^{+576}_{-80}	10.0 ± 5.0	3
σ Ori	150^{+155}_{-76}	20.0 ± 4.0	3
NGC 2068	151^{+169}_{-86}	5.0 ± 3.0	3
NGC 2384	189^{+192}_{-95}	16.5 ± 1.5	3
Mon R2	225^{+236}_{-117}	15.0 ± 5.0	3
IRAS 06073+1249	239^{+242}_{-120}	11.0 ± 4.0	3
Trumpler 24	251^{+291}_{-131}	14.5 ± 2.5	3
IC 5146	293^{+305}_{-226}	14.0 ± 4.0	3
HD 52266	400 ± 350	28.0 ± 3.5	3
HD 57682	400 ± 350	28.0 ± 3.5	3
Alicante 5	461^{+516}_{-234}	12.0 ± 4.0	3
Cep OB3b	485^{+497}_{-243}	37.7 ± 5.0	3
HD 153426	500 ± 350	40.0 ± 6.5	3
NGC 2264	525^{+537}_{-267}	25.0 ± 5.0	3
Sh2-294	525^{+540}_{-267}	12.5 ± 2.5	3
RCW 116B	536^{+557}_{-276}	21.0 ± 5.0	3
NGC 6383	561^{+563}_{-281}	37.7 ± 5.0	3
Alicante 1	577^{+583}_{-290}	45.0 ± 5.0	3
HD 52533	621^{+1077}_{-417}	26.7 ± 3.0	3
Sh2-128	666^{+736}_{-342}	37.7 ± 5.0	3
NGC 2024	690^{+706}_{-350}	20.0 ± 4.0	3
HD 195592	725^{+757}_{-364}	40.0 ± 10.0	3
Sh2-173	748^{+901}_{-395}	25.4 ± 5.0	3
DBSB 48	792^{+1126}_{-416}	56.6 ± 15.0	3
NGC 2362	809^{+823}_{-409}	43.0 ± 7.0	3
Pismis 11	896^{+938}_{-448}	$40.0^{+40.0}_{-0.0}$	3
Taurus-Auriga 5	16	2.5	4
Taurus-Auriga 2	16	3.0	4
Taurus-Auriga 4	18	2.5	4
Lupus 3	18	2.8	4
Cha I 2	20	3.0	4
IC 348 1	126	4.0	4
LkHα 101	195^{+295}_{-123}	$12.3^{+5.7}_{-5.3}$	4
RCW 36	591^{+619}_{-305}	$20.9^{+8.1}_{-6.9}$	4
[BDSB2003] 164	842^{+1065}_{-429}	$32.2^{+20.8}_{-8.2}$	4
[FSR2007] 777	949^{+2166}_{-758}	17.0 ± 5.0	4
NGC 6530	1118^{+1132}_{-564}	$55.5^{+13.5}_{-12.5}$	4
[FSR2007] 734	1175^{+1202}_{-833}	95.0 ± 30.0	4
[DBSB2003] 177	1265^{+1266}_{-633}	$55.5^{+13.5}_{-12.5}$	4
[DB2000] 52	1416^{+1591}_{-724}	$25.1^{+9.9}_{-8.1}$	4
[DB2000] 26	1705^{+1721}_{-852}	$50.4^{+12.6}_{-12.4}$	4
RCW 38	2251^{+2276}_{-1132}	$39.9^{+13.1}_{-11.9}$	4
Mercer 23	3687^{+3793}_{-1859}	$100.0^{+50.0}_{-20.0}$	4
NGC 2103	3853^{+3905}_{-1937}	$85.8^{+34.2}_{-21.8}$	4
NGC 6231	4595^{+4676}_{-2312}	$42.0^{+41.0}_{-8.0}$	4
Westerlund 2	8845^{+9009}_{-4456}	$121.0^{+29.0}_{-43.8}$	4
Danks 2	2900	70^{+15}_{-10}	5, 6
Danks 1	7900	120^{+30}_{-20}	5, 6
RCW 79	3000	$46.1^{+13.3}_{-12.7}$	5, 7
Trumpler 14	10000	127^{+13}_{-27}	8, 9
ρ Oph	100	9	10
ONC	1800	39 ± 6	10
NGC 6611	1630	61^{+14}_{-10}	11, 4
RCW 120	1650	$29.9^{+5.9}_{-6.8}$	7, 12

References. (1) Crowther et al. 2010; (2) Clarkson et al. 2012; (3) Weidner et al. 2010; (4) Weidner et al. 2013; (5) Chené et al. 2012; (6) Davies et al. 2012; (7) Martins et al. 2010; (8) Ascenso et al. 2007; (9) Hur et al. 2012; (10) Crowther 2012; (11) Bonatto et al. 2006; (12) Deharveng et al. 2009.

A very interesting feature of the dispersion in M_{max} determined using the MASSCLEAN simulations should be noted in Figures 5(a) and (b). The range of M_{max} is independent of M_{limit} as long as the mass of the cluster is smaller than the value where the upper stellar mass limit could be reached, i.e., what Kroupa et al. (2011) define to be *unsaturated clusters*. This is a result that would be expected, and we consider it a validation of the MIMFS method. For example, from our *10 million* Monte Carlo simulations, the mass of the most massive star of a 1000 $M_\odot$ cluster is less than 120 $M_\odot$. There is no reason the dispersion in M_{max} for clusters with masses lower than 1000 $M_\odot$ should depend in any way on an M_{limit}, if the limit is higher than 120 $M_\odot$.

Everything from Figure 5(a) is displayed in Figure 5(b), but using a logarithmic scale and including many more observational points representing real clusters. Here it is borne out: the most massive star seen never exceeds the range of values predicted from our simulations over a cluster mass range of nearly two orders of magnitude. Such a relationship can only be proved to exist by studying these low-mass, unsaturated clusters, where the maximum stellar mass is not being limited by any additional, outside stellar physics limit (indicated by an M_{limit} value). Once again, it is obvious that the dispersion in M_{max} is independent of M_{limit} for *unsaturated clusters* and that the upper stellar mass limit should be at least 150 $M_\odot$. Furthermore, Figure 5(b) confirms that clusters with $M_{cluster} < 1000\,M_\odot$ are not affected by the choice of M_{limit} in the 150–1000 $M_\odot$ range. For all of these reasons, low-mass clusters are the ideal candidates to study M_{max}. This is why we included in the figure the observed values for the low-mass clusters from Weidner et al. (2010; green dots). Additional clusters from Weidner et al. (2013) are presented as red dots, and other clusters from the literature are shown as cyan dots. All of these clusters are consistent with the dispersion range of M_{max} we determined.

The Crowther et al. (2010) clusters are presented as red squares in Figure 5, but they are outside the low-mass range, which is our main focus. The *canonical* M_{max}–$M_{cluster}$ relation from our $M_1(M_{limit})$ and Kroupa et al. (2011) are presented as the blue lines (with four different values for M_{limit}) and the single cyan line, respectively. We also include 40 MASSCLEAN clusters, as yellow dots. They will be described in the next section.

For yet another view of the MIMFS simulation results, we present the dispersion range, the difference between the upper and the lower limits of M_{max}, $\Delta M_{max} = M_{max,up} - M_{max,lo}$, in Figure 6(a), for all four values of the M_{limit} discussed above versus the cluster total mass. Since the range of M_{max} is independent of M_{limit} for *unsaturated clusters*, ΔM_{max} is also independent. Figure 6(b) is the same as Figure 6(a), only presented on a logarithmic scale. Figure 6(c) is again the same values, only now we are showing ΔM_{max} as a percentage of $M_{cluster}$, on a logarithmic scale.

5. THE MOST MASSIVE STAR IN STELLAR CLUSTERS DERIVED FROM INTEGRATED MAGNITUDES AND COLORS

The degree to which the integrated colors and magnitudes of stellar clusters can be expected to vary from the mean SSP model prediction is strongly anticorrelated with the cluster's mass (e.g., Popescu & Hanson 2010a, 2010b; Popescu et al. 2012). In other words, the most massive star in a cluster's mass distribution has an increasingly prominent influence in the magnitude and colors of lower mass clusters. It is our goal to exploit this observed dispersion to estimate the mass of the most massive star in a sample of low-mass stellar clusters of known age and mass, using nothing but the integrated broadband magnitudes of the clusters.

To do this, we investigated the variation of *UBV* colors as a function of the mass of the most massive star in the distribution, M_{max}. We performed *25 million* MASSCLEAN Monte Carlo simulations for clusters in the 200–1000 $M_\odot$ range. We used $M_{cluster} = 1000\,M_\odot$ as the upper limit because in this range the dispersion in the maximum stellar mass, M_{max}, is independent of the stellar upper mass limit, M_{limit}. As described in Section 4, these clusters are expected to be *unsaturated*. We used the Kroupa–Salpeter IMF (Equation (3)) and the Padova stellar evolutionary models (Marigo et al. 2008; Girardi et al. 2010), for $Z = 0.008$ metallicity. In this way, we created a special version of the MASSCLEAN*colors* database (Popescu & Hanson 2010b; Popescu et al. 2012) that contains mass, age, and *UBV* but *now also* M_{max} for each cluster.[2]

In Figure 7, we show an example of the variation of M_V, $(B-V)_0$, and $(U-B)_0$ for $M_{cluster} = 200\,M_\odot$. In the three *left* panels, the small dots are color-coded to indicate the maximum mass, M_{max}. Blue, green, yellow, orange, and red show the value of M_{max} for a cluster with the given absolute magnitude and age. The gray region of the diagram is filled with small dots representing clusters that have already lost their most massive star in the distribution as a result of evolution. The *right* three panels are also color-coded but show the ratio between the mass of the most massive star in the distribution and the *canonical value*, $M_{max}/M_1(M_{limit})$. The *canonical value* is displayed in black (ratio = 1.0), and the ±35% values around it are shown in shades of cyan and orange, respectively. Higher values of this ratio are presented in different shades from magenta to dark magenta. All of the clusters that are too old and have already lost their most massive star are again displayed in gray.

The influence of the most massive star on the integrated properties of a cluster is most obvious in Figures 7(a) and (b). For a given age, the integrated magnitude M_V of a low-mass cluster will greatly increase with M_{max}.

Also shown in Figure 7 are nine clusters with masses $M_{cluster} = 200\,M_\odot$ from Popescu et al. (2012). These are given as cyan dots in the left panels and as green dots in the right panels. These clusters have well-constrained age and mass, determined from our mass-dependent SSP MASSCLEAN models (Popescu & Hanson 2010b; Popescu et al. 2012). They were selected to be young enough to still contain their most massive star (i.e., to be on the *colored* part of the plots presented in Figure 7). It can be seen that the clusters' position on the color–age planes presented in Figure 7 is related to the most massive star in the cluster. One can see how this might be used to estimate the value of the most massive star in a cluster of known mass and age, based on an analysis of its broadband colors.

It is with this goal in mind that we created the newest application in the MASSCLEAN package, MASSCLEAN*max*. This application uses yet another, newly created MASSCLEAN*colors* database based on *25 million* simulated clusters. The newest version of the MASSCLEAN*colors* database was built using MASSCLEAN (Popescu & Hanson 2009), the Kroupa IMF (Kroupa 2001), and Padova stellar evolutionary models with $Z = 0.008$ (Marigo et al. 2008). Compared with the previous version of the database (Popescu & Hanson 2010b;

[2] This is the *initial* mass of the most massive star in the distribution, unaffected by the stellar evolution.

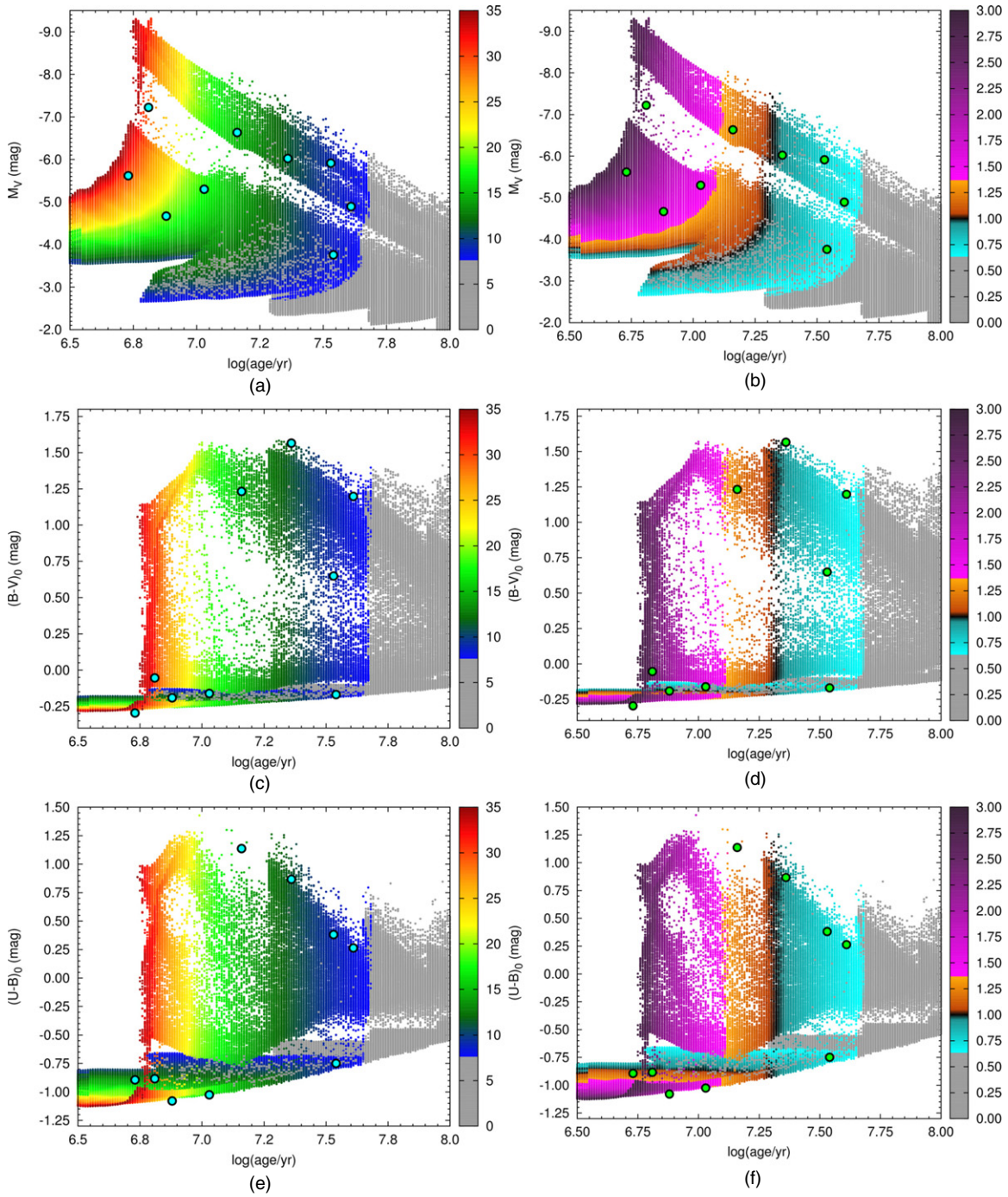

Figure 7. Subset of our *25 million* Monte Carlo simulations, for $M_{cluster} = 200\,M_{\odot}$. The cyan (left) and green (right) dots are MASSCLEAN clusters from Popescu et al. (2012). Left: dots are color-coded to show the integrated color or magnitude of a 200 M_{max} cluster with that M_{max}, the mass of the most massive star, with time. The clusters displayed in gray have already lost their most massive star. Right: dots are color-coded to show the ratio M_{max}/M_1, and the gray clusters have already lost the most massive star.

(A color version of this figure is available in the online journal.)

Popescu et al. 2012), it contains clusters only in the 200–1000 $M_{\odot}$ range and ages in the (6.00–10.13) $\log(age/yr)$ range, and the mass of the most massive star in the distribution, M_{max}, is included. MASSCLEAN*max* then considers the stellar cluster's known mass and age (Popescu et al. 2012), M_V, $(B-V)_0$, and $(U-B)_0$ (Hunter et al. 2003), and using the colors and magnitudes predicted in the database and through probabilistic inference, it finds the most probable value for M_{max} for each cluster.

Values of M_{max} computed by MASSCLEAN*max* for 40 low-mass clusters ($M_{cluster}$ in the 200–1000 $M_{\odot}$ range) are presented in Figure 8 (yellow dots) and listed in Table 2. The 40 MASSCLEAN clusters were selected from the Popescu et al. (2012) catalog to be young and low-mass, so their most massive star will still be present in the mass distribution. The Weidner et al. (2010) clusters, with their maximum mass as derived by them, are presented as green dots and the additional clusters from Weidner et al. (2013) are presented as red dots (unfortunately,

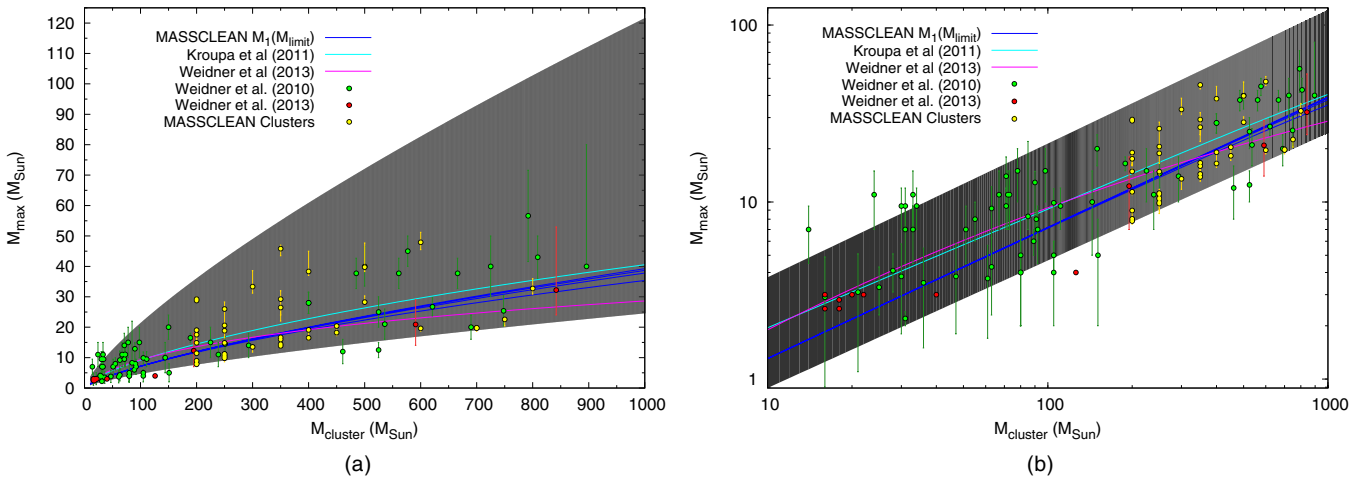

Figure 8. Maximum stellar mass, M_{max}, versus stellar cluster total mass, $M_{cluster}$, similar to Figure 5(b) but concentrating on just the low-mass clusters, $M_{cluster} < 1000\ M_{\odot}$, showing (a) a linear plot and (b) a logarithmic plot. The dark gray region identifies the MASSCLEAN solution for the range of variation of M_{max}. The locations of real clusters from Weidner et al. (2010), from Weidner et al. (2013), and calculated using MASSCLEAN*max* are shown as green, red, and yellow dots, respectively.

(A color version of this figure is available in the online journal.)

the majority of them do not include error bars). Also presented in Figure 8(a), along with our 40 clusters and the Weidner et al. (2010) clusters, is the range of variation of M_{max} as the broad gray area. The *canonical* forms given by $M_1(M_{limit})$, Kroupa et al. (2011), and Weidner et al. (2013) are presented as blue, cyan, and magenta lines, respectively. All sets of yellow, red, and green clusters show a pretty similar placement within the M_{max} range, determined in Section 4. Figure 8(b) is identical to Figure 8(a), but shown on a logarithmic scale. Note that these figures are virtually identical to what was shown in Figure 5(b), only here we have limited the plot to a smaller stellar and cluster mass range.

It is important to remember that the MASSCLEAN*max* method provides only an estimate of M_{max}. Furthermore, it assumes that we have obtained *perfect* values for the age and mass of the cluster under study. However, any age and mass derived for a stellar cluster will have some associated error, no matter what method is used to obtain them. We believe the accuracy with which we can estimate M_{max} would be increased if we were able to include the error bars in age and mass of the cluster under study in the analysis. This will be the subject of future work.

6. ANALYTICAL DESCRIPTION OF M_{max} RANGE AND M_{max}–$M_{cluster}$ RELATION

As described in the previous sections, our MASSCLEAN simulations indicate that the maximum stellar mass in a stellar cluster, M_{max}, covers a range of mass that is dependent on the mass of the cluster. The well-behaved shape of this range presented in Figures 4 and 5 and shaded gray lends itself to finding an analytical form for the upper and lower limits. The logarithmic plot from Figure 5(b) shows that a power law is a good fit for both limits in the case of *unsaturated* clusters.

Optimal sampling (Kroupa et al. 2011) uses a single-valued M_{max}–$M_{cluster}$ relation, computed with a 150 $M_{\odot}$ *canonical limit* and described in a complicated form by Equation (24). On the other hand, hydrodynamical simulations (e.g., Bonnell et al. 2004; Peters et al. 2010, 2011; Kroupa et al. 2011) give the dependence between the mass of the most massive star and cluster's mass in the power-law form

$$M_{max} = 0.39 M_{cluster}^{2/3}. \quad (27)$$

This form corresponds to the best fit to these hydrodynamical simulations, although some scatter might still exist around it (e.g., Bonnell et al. 2004).

From our simulations, we have determined that the M_{max}–$M_{cluster}$ relation is not single valued. The range of variation is best described by an upper (M_{max_1}) and lower (M_{max_2}) limit. These two limits can be written as a power law in a similar form to Equation (27) as

$$M_{max_{1,2}} = k_{1,2} M_{cluster}^{\beta_{1,2}} \quad (28)$$

with $k_1 = 0.66$, $k_2 = 0.17$, $\beta_1 = 0.755$, and $\beta_2 = 0.720$.

The upper and lower limits given by Equation (28) are presented in Figure 9(a) as the orange and purple lines, respectively. The M_{max}–$M_{cluster}$ relation determined from hydrodynamical simulations (Equation (27)) is presented as the white line. The range of M_{max} variation is presented as the gray area. The MASSCLEAN clusters, Weidner et al. (2010) clusters, and Weidner et al. (2013) are presented as yellow, green, and red dots, respectively, similarly to Figure 8(b).

In Figure 9(b), we extend both the $M_{cluster}$ and M_{max} ranges. $M_{\max_{1,2}}$ are presented as green, blue, black, and red lines for $M_{limit} = 150$, 300, 500, and 1000 $M_{\odot}$, respectively. We note that the $M_{max_{1,2}}$ limits given by Equation (28) stand for unsaturated clusters, regardless of the M_{limit}. In addition to MASSCLEAN clusters, Weidner et al. (2010) clusters, and Weidner et al. (2013) clusters, we also show Crowther et al. (2010) clusters as red squares, and other clusters from the literature as cyan dots.

Based on the fact that M_{max} is related to the value of α_3 (Equations (17), (20), and (22)), just to emphasize this dependence, Equation (28) could be rewritten as

$$M_{max_{1,2}} = k_{1,2} M_{cluster}^{\frac{1}{\alpha_3 - 1 \mp \delta_{1,2}}} \quad (29)$$

with $\delta_1 = 0.0255$, $\delta_2 = 0.0388$, and $\alpha_3 = 2.35$.

Table 2
LMC Clusters with Values of M_{max}

	Integrated Photometry (Hunter et al. 2003)				MASSCLEAN		
Name(s)	M_V	$(U-B)_0$	$(B-V)_0$	$(V-R)_0$	Age[a]	Mass[a]	M_{max}[b]
	(*mag*)	(*mag*)	(*mag*)	(*mag*)	(*log*)	($M_\odot$)	($M_\odot$)
1	2	3	4	5	6	7	8
BSDL2208	-5.618 ± 0.012	-0.894 ± 0.005	-0.296 ± 0.012	-0.086 ± 0.026	6.73	200	$29.24^{+0.76}_{-0.74}$
NGC 1837.SL217	-7.223 ± 0.004	-0.884 ± 0.002	-0.054 ± 0.004	-0.036 ± 0.009	6.81	200	28.76 ± 0.01
KMHK263	-4.671 ± 0.021	-1.079 ± 0.006	-0.191 ± 0.021	-0.167 ± 0.057	6.88	200	$19.02^{+0.38}_{-3.02}$
BSDL579	-5.300 ± 0.011	-1.025 ± 0.004	-0.161 ± 0.011	-0.088 ± 0.027	7.03	200	$17.54^{+0.71}_{-1.34}$
KMHK612	-6.634 ± 0.005	1.137 ± 0.005	1.232 ± 0.007	0.585 ± 0.008	7.16	200	$14.88^{+3.37}_{-0.18}$
BSDL2119	-6.023 ± 0.008	0.867 ± 0.011	1.566 ± 0.013	0.875 ± 0.011	7.36	200	$11.43^{+0.07}_{-0.43}$
SL294.KMHK627	-5.914 ± 0.032	0.381 ± 0.024	0.649 ± 0.037	0.182 ± 0.060	7.53	200	$8.96^{+0.14}_{-0.11}$
BSDL499	-3.761 ± 0.039	-0.749 ± 0.011	-0.169 ± 0.039	-0.186 ± 0.105	7.54	200	$7.80^{+0.90}_{-0.30}$
OGLE-LMC0297	-4.894 ± 0.027	0.264 ± 0.043	1.198 ± 0.047	0.627 ± 0.039	7.61	200	$8.04^{+0.26}_{-0.05}$
BSDL137	-5.099 ± 0.014	-1.223 ± 0.004	-0.270 ± 0.014	-0.080 ± 0.033	6.68	250	$26.00^{+2.30}_{-6.00}$
BSDL2215	-5.718 ± 0.010	-0.991 ± 0.003	-0.198 ± 0.010	-0.083 ± 0.024	6.95	250	$20.58^{+0.62}_{-1.98}$
BSDL2704	-5.473 ± 0.013	-1.029 ± 0.005	-0.140 ± 0.013	-0.035 ± 0.028	7.00	250	$18.85^{+0.35}_{-2.35}$
BSDL358	-6.681 ± 0.006	0.872 ± 0.007	1.167 ± 0.009	0.753 ± 0.008	7.18	250	$14.84^{+0.06}_{-0.64}$
KMHK900	-4.448 ± 0.018	-0.883 ± 0.006	-0.195 ± 0.018	-0.021 ± 0.047	7.31	250	$10.54^{+1.26}_{-0.54}$
BSDL1760	-4.351 ± 0.020	-0.868 ± 0.006	-0.246 ± 0.020	-0.045 ± 0.053	7.34	250	$10.40^{+0.90}_{-1.00}$
OGLE-LMC0169	-6.335 ± 0.008	0.607 ± 0.008	0.803 ± 0.011	0.471 ± 0.013	7.36	250	$11.22^{+0.18}_{-0.22}$
BSDL917	-6.279 ± 0.007	0.502 ± 0.005	0.878 ± 0.008	0.421 ± 0.012	7.37	250	$11.07^{+0.23}_{-0.27}$
BSDL256	-4.329 ± 0.035	-0.811 ± 0.012	-0.227 ± 0.035	-0.170 ± 0.087	7.41	250	$9.80^{+0.52}_{-0.74}$
BSDL25	-4.267 ± 0.030	-0.795 ± 0.010	-0.210 ± 0.030	-0.226 ± 0.079	7.42	250	$9.94^{+0.26}_{-1.34}$
BSDL295	-6.303 ± 0.008	-0.927 ± 0.003	-0.268 ± 0.008	-0.133 ± 0.018	6.72	300	$33.34^{+5.26}_{-2.14}$
BSDL2448	-4.790 ± 0.022	-0.934 ± 0.008	-0.116 ± 0.022	-0.001 ± 0.053	7.20	300	$13.52^{+0.38}_{-1.72}$
KMHK237	-6.638 ± 0.006	-0.979 ± 0.002	-0.259 ± 0.006	-0.143 ± 0.014	6.60	350	$45.84^{+1.16}_{-2.34}$
BCD1	-5.786 ± 0.016	-0.893 ± 0.007	-0.260 ± 0.017	-0.062 ± 0.032	6.73	350	$29.23^{+2.77}_{-7.23}$
BSDL2883	-6.303 ± 0.007	-1.011 ± 0.002	-0.127 ± 0.007	-0.058 ± 0.015	6.84	350	$26.45^{+0.55}_{-2.45}$
BSDL349	-5.910 ± 0.010	-0.841 ± 0.003	-0.152 ± 0.010	-0.062 ± 0.015	7.08	350	$16.65^{+0.15}_{-1.35}$
BSDL34	-5.936 ± 0.010	-0.835 ± 0.004	-0.123 ± 0.010	-0.038 ± 0.023	7.11	350	$15.96^{+0.04}_{-0.96}$
BSDL2487	-5.497 ± 0.023	-0.831 ± 0.008	-0.106 ± 0.023	-0.016 ± 0.043	7.20	350	$13.87^{+0.03}_{-0.77}$
HS59.KMHK253	-6.843 ± 0.005	0.597 ± 0.004	0.845 ± 0.006	0.417 ± 0.008	7.20	350	$14.40^{+0.10}_{-0.60}$
BSDL1834	-7.016 ± 0.005	-1.040 ± 0.002	-0.072 ± 0.005	0.067 ± 0.010	6.69	400	$38.32^{+6.68}_{-1.32}$
BSDL2614	-5.618 ± 0.012	-0.988 ± 0.005	-0.176 ± 0.012	-0.136 ± 0.028	7.00	400	$19.11^{+0.14}_{-3.11}$
SL563	-6.113 ± 0.012	-0.810 ± 0.004	-0.137 ± 0.012	-0.047 ± 0.024	7.09	400	$16.50^{+0.10}_{-0.80}$
BSDL2725	-6.354 ± 0.006	-0.955 ± 0.002	-0.087 ± 0.006	-0.069 ± 0.013	6.96	450	$20.39^{+0.36}_{-1.89}$
BSDL2720	-6.230 ± 0.007	-0.883 ± 0.003	-0.034 ± 0.007	0.006 ± 0.015	7.03	450	$18.24^{+0.06}_{-1.04}$
H88-266	-7.077 ± 0.009	-1.055 ± 0.004	-0.206 ± 0.009	-0.064 ± 0.017	6.67	500	$39.74^{+7.96}_{-1.44}$
HS245	-8.496 ± 0.002	0.559 ± 0.003	1.172 ± 0.003	0.472 ± 0.004	6.82	500	$28.23^{+2.07}_{-0.23}$
BSDL305	-7.801 ± 0.004	-0.941 ± 0.002	-0.083 ± 0.004	-0.015 ± 0.008	6.63	600	$47.90^{+3.30}_{-2.40}$
BSDL2721	-6.393 ± 0.008	-0.967 ± 0.003	-0.050 ± 0.008	-0.004 ± 0.017	6.98	600	$19.62^{+0.28}_{-0.92}$
BSDL2583	-6.081 ± 0.009	-0.960 ± 0.003	-0.184 ± 0.009	-0.106 ± 0.020	6.98	700	$19.66^{+0.24}_{-0.96}$
HS74	-6.560 ± 0.009	-0.844 ± 0.003	-0.210 ± 0.009	0.035 ± 0.020	6.98	700	$19.83^{+0.07}_{-0.83}$
KMHK339	-6.396 ± 0.008	-0.952 ± 0.003	-0.158 ± 0.008	-0.068 ± 0.020	6.92	750	$22.56^{+0.04}_{-2.16}$
NGC 2102.SL665	-7.509 ± 0.004	-0.879 ± 0.002	-0.118 ± 0.004	-0.080 ± 0.010	6.76	800	$32.73^{+3.27}_{-1.83}$

Notes.
[a] Popescu et al. (2012).
[b] This work.

Regardless of the way the dependence is written, we find that the M_{max}–$M_{cluster}$ relation for unsaturated clusters is described by the upper and lower limits $M_{max_{1,2}}$. Both of these values correspond to power laws of the mass of the cluster and are independent of any particular value for M_{limit} when applied to unsaturated, low-mass stellar clusters.

7. SUMMARY AND CONCLUSION

The IMF is one of the most fundamental of astrophysical distribution functions, with broad applicability. Traditionally, the IMF functional form was predominantly used to fit observational data. However, in current investigations, simulated data

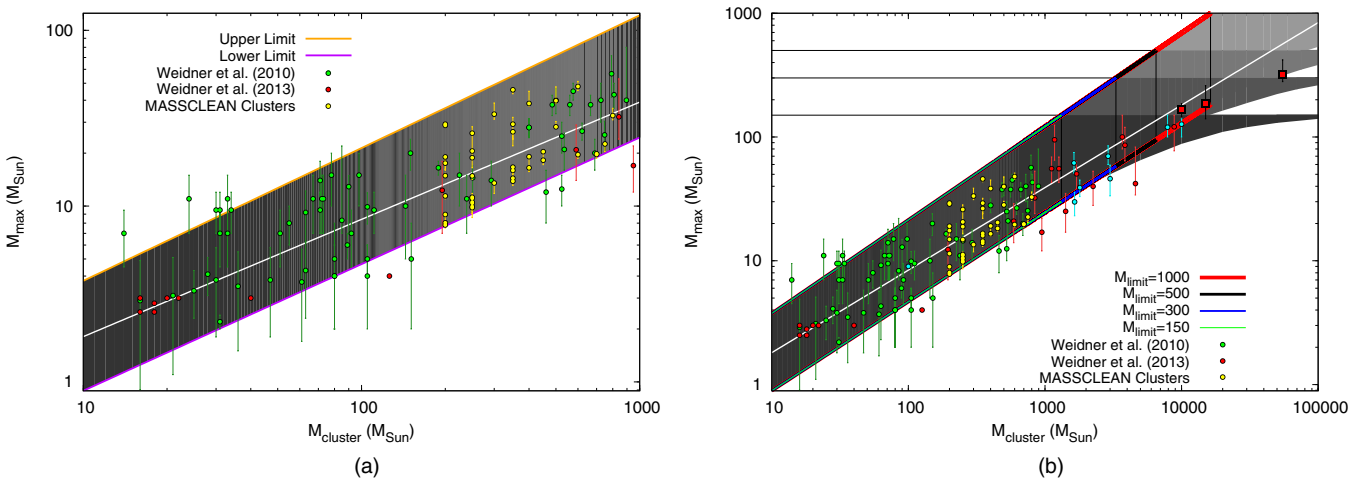

Figure 9. (a) Same as Figure 8(b), but showing our analytical fit to the gray regions' upper and lower limits. The white line presents results from hydrodynamical simulations. (b) Similar to (a), but extending to a larger cluster mass and including the effect of applying an upper mass limit, M_{limit}. Crowther et al. (2010) clusters are presented as red squares, and additional clusters from the literature are shows as cyan dots.

(A color version of this figure is available in the online journal.)

are becoming increasingly important. This warrants careful consideration that the methods used for filling an IMF distribution in such applications are done correctly. The most often used (and convenient) way to do this, through random sampling, does not properly fill an IMF distribution, as described by Kroupa et al. (2011).

Optimal sampling (Kroupa et al. 2011) does fill the IMF correctly. But because it allows for multiple stars per mass bin, it lacks a certain resolution to pursue additional fundamental questions about the distribution. Moreover, it leads to a single-valued M_{max}–$M_{cluster}$ relation. Kroupa et al. (2011) attempt to explain the range observed in this relationship (our Figures 5(b), 8, and 9, and their Figures 4 and 5) as due to observational error and stochastic variations in the intrinsic precluster cloud conditions, which may vary a single-valued M_{max}–$M_{cluster}$ relation. We presented our MASSCLEAN IMF sampling (MIMFS) method, which is able to properly fill the IMF using just one star per mass bin and requires no assumption about the M_{max}–$M_{cluster}$ relation or M_{limit}.

From our *10 million* MASSCLEAN Monte Carlo simulations, we determined the expected mass range of the most massive star in the stellar mass distribution as a function of the mass of the cluster. As a check on these simulations, we confirmed that this maximum mass range is independent of M_{limit} for *unsaturated* clusters. What is particularly validating about our method is it *predicts* the M_{max}–$M_{cluster}$ relation to be a range, not single valued. It even predicts the correct upper and lower mass range when compared with real clusters.

We described our method to determine M_{max} from *UBV* integrated colors and magnitudes using *25 million* MASSCLEAN Monte Carlo simulations. With it, we estimate the maximum stellar mass for 40 LMC clusters. These values of maximum stellar mass, relative to the cluster total mass, are consistent with previous determinations using different methods on other similar-mass stellar clusters (e.g., Weidner et al. 2010).

Finally, we provided an analytical, power-law description of the M_{max} range, which enabled us to cleanly describe the M_{max}–$M_{cluster}$ relation. For *unsaturated clusters*, the M_{max}–$M_{cluster}$ relation is not single valued. It is described by an *upper* and *lower* limit. Both of these limits correspond to power-law functions of the stellar cluster mass, $M_{cluster}$, and are independent of M_{limit} for *unsaturated* clusters. Such a relationship is consistent with previous results from hydrodynamical simulations.

We thank the referee for useful comments and suggestions. We are grateful for suggestions made on an early draft of this work by Bruce Elmegreen and Søren Larsen. Their ideas led to significant improvements in the presentation. This material is based upon work supported by the National Science Foundation under grants AST 0607497 and AST 1009550 to the University of Cincinnati. B.P. acknowledges additional support from CMP.

REFERENCES

Ascenso, J., Alves, J., Vicente, S., & Lago, M. T. V. T. 2007, A&A, 476, 199
Banerjee, S., Kroupa, P., & Oh, S. 2012a, MNRAS, 426, 1416
Banerjee, S., Kroupa, P., & Oh, S. 2012b, ApJ, 746, 15
Baraffe, I., Heger, A., & Woosley, S. E. 2001, ApJ, 550, 890
Bonatto, C., Santos, J. F. C., Jr., & Bica, E. 2006, A&A, 445, 567
Bonnell, I. A., Vine, S. G., & Bate, M. R. 2004, MNRAS, 349, 735
Bruzual, G., & Charlot, S. 2003, MNRAS, 344, 1000
Chené, A. N., Borissova, J., Clarke, J. R. A., et al. 2012, A&A, 545, 54
Clarkson, W. I., Ghez, A. M., Morris, M. R., et al. 2012, ApJ, 751, 132
Crowther, P. A. 2012, in IAU Symp. 279, Death of Massive Stars: Supernovae and Gamma-Ray Bursts, ed. P. W. A. Roming, N. Kawai, & E. Pian (Cambridge: Cambridge Univ. Press), 9
Crowther, P. A., Schnurr, O., Hirschi, R., et al. 2010, MNRAS, 408, 731
Davies, B., Clark, J. S., Trombley, C., et al. 2012, MNRAS, 419, 1871
Deharveng, L., Zavagno, A., Schuller, F., et al. 2009, A&A, 496, 177
Elmegreen, B. G. 2000, ApJ, 539, 342
Elmegreen, B. G. 2004, MNRAS, 354, 367
Figer, D. F. 2005, Natur, 434, 192
Girardi, L., Williams, B. F., Gilbert, K. M., et al. 2010, ApJ, 724, 1030
Herrero, A., Kudritzki, R. P., Vilchez, J. M., et al. 1992, A&A, 261, 209
Hunter, D. A., Elmegreen, B. G., Dupuy, T. J., & Mortonson, M. 2003, AJ, 126, 1836
Hur, H., Sung, H., & Bessell, M. S. 2012, AJ, 143, 41
Kroupa, P. 2001, MNRAS, 322, 231
Kroupa, P. 2002, Sci, 295, 82
Kroupa, P., Weidner, C., Pflamm-Altenburg, J., et al. 2011, in Planets, Stars and Stellar Systems, ed. T. D. Oswalt & G. Gilmore (Dordrecht: Springer Science+Business Media), 115
Maíz Apellániz, J. 2009, ApJ, 699, 1938
Maíz Apellániz, J., & Úbeda, L. 2005, ApJ, 629, 873
Marigo, P., Girardi, L., Bressan, A., et al. 2008, A&A, 482, 833
Martins, F., Pomarès, M., Deharveng, L., Zavagno, A., & Bouret, J. C. 2010, A&A, 510, 32

Massey, P. 2011, in ASP Conf. 440, UP2010: Have Observations Revealed a Variable Upper End of the Initial Mass Function? ed. M. Treyer, T. K. Wyder, J. D. Neill, M. Seibert, & J. C. Lee (San Francisco, CA: ASP), 29
Oey, M. S., & Clarke, C. J. 2005, ApJL, 620, L43
Peters, T., Klessen, R. S., Mac Low, M.-M., & Banerjee, R. 2010, ApJ, 725, 134
Peters, T., Klessen, R. S., Mac Low, M.-M., & Banerjee, R. 2011, in Stellar Clusters & Associations: A RIA Workshop on Gaia, ed. A. Navarro (Granada: ESF)
Popescu, B., & Hanson, M. M. 2009, AJ, 138, 1724
Popescu, B., & Hanson, M. M. 2010a, ApJL, 713, L21
Popescu, B., & Hanson, M. M. 2010b, ApJ, 724, 296
Popescu, B., Hanson, M. M., & Elmegreen, B. G. 2012, ApJ, 751, 122
Salpeter, E. E. 1955, ApJ, 121, 161
Sana, H., van Boeckel, T., Tramper, F., et al. 2013, MNRAS, 432, L26
Selman, F., Melnick, J., Bosch, G., & Terlevich, R. 1999, A&A, 347, 532
Stothers, R. 1992, ApJ, 392, 706
Weidner, C., & Kroupa, P. 2004, MNRAS, 348, 187
Weidner, C., Kroupa, P., & Bonnell, I. A. D. 2010, MNRAS, 401, 275
Weidner, C., Kroupa, P., & Pflamm-Altenburg, J. 2013, MNRAS, 434, 84